

ROBUST ENDMEMBER EXTRACTION IN THE PRESENCE OF ANOMALIES

O Duran and M Petrou

Imperial College London, Dept. of Electrical and Electronic Engineering,
Exhibition Road, South Kensington, London, SW7 2AZ
United Kingdom
email: maria.petrou@imperial.ac.uk

ABSTRACT

Most available methods for endmember extraction use the convexity of the data structure and consider the vertices of the data as the purest pixels. Such methods do not consider the applicability of the linear mixing model once the endmembers have been extracted. Thus they might return false endmembers if the data contain outliers such as anomalies. In this paper we tackle this problem by identifying endmembers in a robust way, separating them from outliers. We tested the proposed algorithm with real and synthetic data and compared it with the VCA, SGA and N-FINDR algorithms, showing better and more robust endmember extraction.

1. INTRODUCTION

Spectral unmixing consists of decomposing the measured spectrum of a mixed pixel into a set of pure class spectra, or *endmembers*, and computing their corresponding fractions, or *abundances*. Pure cover classes correspond to the usual components in the scene, such as water, soil, or metal. Pure substances might be considered rare events in an image where most of the background pixels correspond to mixtures of pure materials.

State of the art endmember extraction methods use the convexity of the data structure and treat the vertices of the data as the purest pixels [1]. The major objection to such methods is that they simply treat the spectra as mathematical vectors, and they do not consider the applicability of the linear model once the endmembers have been extracted. It has to be taken into account that anomalies as well as the purest pixels present in an image might be the extremes of the spread of spectral signatures [2]. In other words, pixels that constitute the vertices of the convex hull of the cloud of data points might be either anomalies or purest pixels, and in order to distinguish between those, the applicability of the linear model has to be considered. On the other hand, methods that search for anomalies might wrongly return endmembers as anomalies, since both populations are relatively small [1].

A robust endmember extraction algorithm for hyperspectral data is presented in this paper. The algorithm extends the

work presented in [3] and shows its applicability for the robust identification of the endmembers in a scene. The method is based on the assumptions that the linear mixing model is valid and that due to the resolution of the image, most pixels are mixtures of relatively rare pure substances. Thus, if we represent all pixels as linear combinations of the background classes, pixels corresponding to each pure class are expected to show extreme abundance values with respect to one of the background classes. They are also expected to show small values of residual error after having applied the unconstrained linear unmixing model (allowing negative and superunity abundances). Anomalies are identified as pixels with spectra that cannot be explained as linear combinations of the spectra of the background classes.

This paper is organised as follows. In Section 2, endmember extraction methods are briefly reviewed. In Section 3, we present the proposed methodology. In Section 4, results are presented. Finally, we conclude in Section 5.

2. ENDMEMBER EXTRACTION TECHNIQUES

Many algorithms have been developed for endmember extraction in hyperspectral data. Some methods use the convexity of the data structure and try to find a set of vertices that represent the endmembers. N-FINDR attempts to find the simplex of maximum volume that can be inscribed within the data set with a given number of vertices [4] [5]. The volume $V(E)$ is calculated as

$$V(E) = \frac{1}{(n-1)!} |\det E| \quad (1)$$

where n is the number of desired endmembers, and E is defined as

$$E \equiv \begin{bmatrix} 1 & 1 & \dots & 1 \\ \mathbf{e}_1 & \mathbf{e}_2 & \dots & \mathbf{e}_n \end{bmatrix} \quad (2)$$

where \mathbf{e}_i are the spectra of the endmembers, represented as column vectors. The procedure begins with a random set of n pixels as endmembers. Then, a trial volume is calculated for every pixel in each endmember position by replacing that endmember and recalculating the volume. If the replacement

results in an increase in volume, the pixel replaces the endmember. This procedure is repeated until there are no more replacements of endmembers. The computational performance of the algorithm depends on the accuracy of the initial random selection of endmembers [6].

The simplex growing algorithm (SGA) [1] improves the N-FINDR algorithm by including a process of growing a simplex by one vertex at a time, until it reaches a desired number of vertices. The virtual dimensionality (VD) [7] is implemented as a stopping rule that determines the number of vertices that have to be generated by the algorithm. Additionally, it also selects an appropriate initial spectrum as the first vertex of the simplex, instead of using random spectra as endmembers for initialisation.

Vertex component analysis (VCA) follows a different approach for endmember extraction. VCA iteratively projects data onto a direction orthogonal to the subspace spanned by the endmembers already determined [8]. The new endmember signature corresponds to the extreme of the projection. The algorithm iterates until the number of expected endmembers is reached.

The major objection to such methods is that when one identifies the extreme pixels in a set as the purest pixels, one may easily include outlier spectra, which do not correspond to the cover classes that make up the observed mixtures. Pixels that constitute the vertices of the convex hull of the cloud of data points might be either anomalies or pure cover class pixels [2], and in order to distinguish between those, the use of a robust method based on the mixing model is needed.

3. METHODOLOGY

The proposed robust unconstrained linear unmixing (RULU) endmember extraction algorithm consists of three steps. In the first stage of the algorithm, the classes associated with the background, which are the dominant classes in the image, are identified by clustering the image pixels [3]. The resulting clusters may be considered as representatives of the background classes in the image. Once the background classes have been determined, we use the unconstrained least square error approach to unmix all pixels in the image. This method estimates the abundance of each component inside the pixel by minimising the sum of the squares of the errors, using as endmembers the background classes. Finally, we search for pixels with extreme values of abundance fractions and low residual error, when expressed as linear combinations of the background class spectra.

To help visualise our ideas, let us consider the spectral space of figure 1. Let us say that the vast majority of the observed spectra may be clustered in three clusters with mean spectra \mathbf{b}_1 , \mathbf{b}_2 and \mathbf{b}_3 . However, in the image one may also observe a few pixels with spectra \mathbf{a}_1 and \mathbf{a}_2 . A non robust algorithm will consider as endmembers the extrema of the convex hull of all

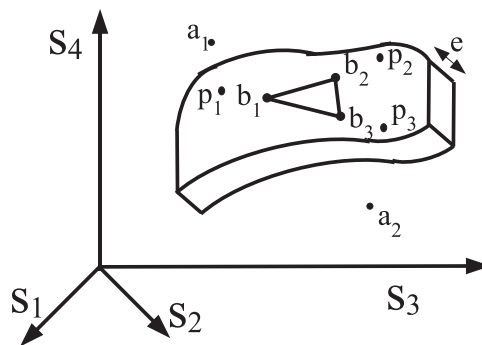


Fig. 1. Manifold in a 4-band space with three background classes, \mathbf{b}_1 , \mathbf{b}_2 and \mathbf{b}_3 . Here, e is the error we are prepared to tolerate for the linear mixing model, and \mathbf{p}_1 , \mathbf{p}_2 and \mathbf{p}_3 are the pure classes, while \mathbf{a}_1 and \mathbf{a}_2 are two anomalies.

observed spectra, including \mathbf{a}_1 and \mathbf{a}_2 . The pure class spectra, however, that gave rise to the observed mixtures, must have spectra that lie on the manifold defined by the mixtures and be expressible in terms of the mixtures with mixing proportions that are negative and/or larger than 1 (i.e. in the particular example of figure 1, they should not lie inside triangle $\mathbf{b}_1 \mathbf{b}_2 \mathbf{b}_3$). In the case of real data, the identified background classes define a low dimensionality manifold embedded in the high dimensionality spectral space. We “thicken” that manifold by allowing pixels to belong to it, as long as their distance from it is below a certain threshold, and we consider all other pixels as anomalies, and thus exclude them from the process of endmember identification. This is done by thresholding the residual error, E_{res} , after having applied the unconstrained linear unmixing model. E_{res} is computed as,

$$E_{res} = \left\| \mathbf{r} - B\hat{\mathbf{f}} \right\| \quad (3)$$

where \mathbf{r} is the spectrum of the pixel, $\hat{\mathbf{f}}$ is the vector of proportions of the background classes, B , that are obtained from the least square error solution of $\mathbf{r} = B\mathbf{f}$. We threshold E_{res} with the error we are prepared to tolerate. This is done in an automatic way using the histogram of the residual error values. Pixels showing extreme abundance values, but residual error smaller than the computed threshold, when expressed as linear combinations of the background class spectra, correspond to the pure classes. On the contrary, pixels that are not compatible with the data (i.e. show residual error higher than the threshold) are considered as anomalies (i.e. rare or unexpected spectra which do not correspond to the pure classes that created the observed mixtures).

Table 1. Spectral angle distance between the extracted endmembers and laboratory reflectances (in degrees) for the RULU, N-FINDR, SGA AND VCA algorithms.

	Substance			
	Alunite	Buddingtonite	Calcite	Kaolinite
RULU	4.8	4	5.6	7.7
N-FINDR	8.5	4.1	5.7	9.9
SGA	4.8	4.5	5.9	7.7
VCA	5.1	5.6	5.8	7.7

4. EXPERIMENTS

4.1. Endmember extraction

To evaluate the performance of the four algorithms (RULU, SGA, VCA and N-FINDR), the similarity of the extracted endmembers with the ground truth endmembers was measured by computing the cosine of the angle between the endmember and the corresponding ground truth spectrum (SAD, spectral angle distance).

The data, used to determine how well the algorithms find the endmembers in the scene, consist of a real AVIRIS hyperspectral image from the Cuprite mining district in Nevada [9]. This image has been widely used to study endmember extraction [6][1]. The 350×350 pixels image has 224 spectral bands with $10 - nm$ spectral resolution. However, bands 1 – 3, 105 – 115, and 150 – 170 were removed prior to the analysis due to water absorption and low SNR in those bands [1] leaving a total of 189 bands. There are a large number of minerals present in this scene but we concentrated our study on four minerals, namely Kaolinite, Buddingtonite, Alunite, and Calcite, that are found to be prominent and in pure form in this area [6]. This data set is particularly well suited to test the background class extraction method, since there are spectral libraries with all the minerals in the scene, that can be used as ground truth.

The virtual dimensionality (VD) criterion [7] is implemented as a stopping rule to determine the number of vertices required for the VCA, SGA and N-FINDR algorithms. We used $VD = 22$ based on the false alarm rate fixed at probability 10^{-4} as it was chosen in [1]. In order to compare RULU with the other methods, we select the number of nodes of the SOM so that the number of clusters is similar to the chosen VD.

Table 1 compares the spectral angles between the extracted endmembers and laboratory reflectances for the four algorithms. RULU performs from marginally better to better than the other algorithms. It is also observed that the RULU and SGA algorithms find the same pixels as endmembers for the Alunite and Kaolinite substances. N-FINDR has the worst performance.

4.2. Robustness in the presence of anomalies

The data used for this experiment consist of 10 hyperspectral images covering 8–11 μm of the spectrum in 30 bands and 128×128 pixels [10]. The scenario contains fields, roads, buildings, trees, pylons, telegraph poles and other features. The anomalies are the materials corresponding to coaches, cows, tractors and landrovers. The pixel size is $16 \times 16m^2$. The sizes of the anomalies are $2.5m \times 10.2m$, $1m \times 3, 3m$, $2.5m \times 8.2m$ and $1.85m \times 4.3m$ for the coach, cow, tractor and landrover, respectively. According to the ground truth, each image is made up from around 50 pure classes. Note that the proposed methodology needs the number of endmember classes to be smaller than the number of available bands, so that the manifold of the background classes is embedded inside the spectral space [3]. In this data set, there are only 30 bands and so, the best we can do is to select 30 nodes for the SOM algorithm, aiming at identifying only the 30 most significant endmembers.

The endmember extraction accuracy is evaluated by comparing estimated abundance fractions by the algorithms with the existing ground-truth abundance maps. The ground truth spectra are extracted for each material from the images themselves by computing the mean spectrum of all pixels that have maximum abundance value for that material.

Table 2 shows the results for one of the images of this data set. Due to the large number of classes, we present the results for the five most prominent endmembers (lawn grass, dry grass, limestone rock, lake sand and black sand) and for all the anomalies (named anomaly 1 to anomaly 7). The first four columns show the estimate of the relative abundance of the endmember corresponding to each material. Ideally, the algorithms should not identify the anomalies as endmembers. If an algorithm performs well and does not mistake an anomaly as endmember, we show in the corresponding line in table 2 an estimate of 0 for that material. On the other hand, the algorithms should identify the purest pixel (ideally estimated abundance 1) for each one of the endmembers. However, note that we present the results for the most prominent materials in the scene, regardless of whether they are present in pure or mixed form. So, for some materials, there might not be a pixel with abundance value 1 in the image. To show the maximum value that the algorithms may estimate for each material, their ground truth maximum abundance fraction is also shown in the tables. Those are the best possible values that the algorithms may identify for each endmember. Note that the pure pixels and anomalies are both rare in the data. RULU exceeds the other algorithms by identifying all the anomalies. RULU identifies the best pixels as endmembers, i.e. it identifies the pixels with larger abundance values with respect to the other methods for three out of the six materials, while VCA identifies the best pixel for the “paved concrete” and SGA for “lake sand” materials. RULU is the only method to find an acceptable estimate for “limestone rock”.

Table 2. Assessment of the endmembers identified by RULU, SGA, VCA and N-FINDR algorithms, respectively. The first four columns show the estimated endmember relative abundance corresponding to each material. The ground truth maximum abundances are shown in the last column.

Material	Estimated abundance				Maximum abundance
	RULU	SGA	VCA	N-FINDR	
Lawn grass	1	1	0.2169	1	1
Dry grass	0.9046	0.9046	0.7864	0.7398	0.9046
Paved concrete	0.9956	0.9814	1	0.9995	1
Limestone rock	0.6655	0.1343	0.3081	0.0861	0.6818
Lake sand	0.8664	0.8825	0.7532	0.8664	0.8825
Black sand	0.9121	0.9121	0.9121	0.6757	0.9234
Anomaly 1	0.1564	0.6006	0.6006	0.6006	1
Anomaly 2	0	1	1	1	1
Anomaly 3	0	1	1	1	1
Anomaly 4	0	1	1	1	1
Anomaly 5	0	1	1	1	1
Anomaly 6	0	0	0	0	1
Anomaly 7	0	1	1	1	1

5. CONCLUSIONS

In this paper, we proposed a new algorithm for the robust identification of endmembers (RULU) in hyperspectral images. The proposed algorithm exploits the fact that endmembers occupy the vertices of the simplex of the data cloud but takes also into account the ability of the linear model to explain the identified spectra. The method is based on unconstrained spectral unmixing to achieve a robust detection. The algorithm assumes the presence of pure pixels in the data, the signatures of which correspond to the extreme values of abundances for the background classes. First, the image pixels are clustered to identify the background classes. Then, the image pixels are unmixed using the unconstrained linear method. Pixels showing extreme abundance values, but small residual error, when expressed as linear combinations of the background class spectra, correspond to the pure classes. On the contrary, pixels showing high residual error are considered as anomalies. It is this last step, where the values of the residual errors are computed, that allows us to characterise the algorithm as robust, as opposed to just using an algorithm that identifies the extreme points of the simplex of data in the spectral space. We tested the method with real and synthetic data and compared it with the VCA, SGA and N-FINDR methods, showing better and robust endmember extraction.

6. ACKNOWLEDGEMENTS

This work has been carried out with the support of General Dynamics UK Ltd and the UK MOD Data and Information Fusion Defence Technology Centre under project DIF DTC

9.3. We thank QinetiQ Ltd for providing the synthetic data set.

7. REFERENCES

- [1] C.-I. Chang, C.-C. Wu, W. Liu, and Y.-C. Ouyang, "A new growing method for simplex-based endmember extraction algorithm," *IEEE Transactions on Geoscience and Remote Sensing*, vol. 44, no. 10, pp. 2804–2819, Oct. 2006.
- [2] B. Penn, "Using self-organizing maps for anomaly detection in hyperspectral imagery," in *IEEE Aerospace Conference Proceedings*, vol. 3, 2002, pp. 1531–1535.
- [3] O. Duran and M. Petrou, "Spectral unmixing with negative and superunity abundances for subpixel anomaly detection," *IEEE Geoscience and Remote Sensing Letters*, vol. 6, no. 1, pp. 152–156, 2009.
- [4] M. E. Winter, "N-FINDR: an algorithm for fast autonomous spectral end-member determination in hyperspectral data," in *Proceedings of SPIE, Volume 3753: Imaging Spectrometry*, vol. 10, 1999.
- [5] M. E. Winter and E. Winter, "New developments in the N-FINDR algorithm," in *IGARSS 2001 International Geoscience and Remote Sensing Symposium*, vol. 1. Sydney, Australia: Springer, aug 2001, pp. 951–956.
- [6] A. Plaza, P. Martinez, R. Perez, and J. Plaza, "Spatial/spectral endmember extraction by multidimensional morphological operations," *IEEE Transactions on Geoscience and Remote Sensing*, vol. 40, no. 9, pp. 2025–2041, 2002.
- [7] C.-I. Chang and Q. Du, "Estimation of number of spectrally distinct signal sources in hyperspectral imagery," *IEEE Transactions on Geoscience and Remote Sensing*, vol. 42, no. 3, pp. 608–619, March 2004.
- [8] J. Nascimento and J. Dias, "Vertex component analysis: a fast algorithm to unmix hyperspectral data," *IEEE Transactions on Geoscience and Remote Sensing*, vol. 43, no. 4, pp. 898–910, April 2005.
- [9] R. N. Clark, G. A. Swayze, R. Wise, K. E. Livo, T. M. Hoefen, R. F. Kokaly, and S. J. Sutley, "USGS digital spectral library splib05a, USGS open file report 03-395," 2003, URL: <http://speclab.cr.usgs.gov/spectral-lib.html>. Last accessed: 09 June 2009.
- [10] M. Nicholas, M. James, and J. Nothard, "Hyperspectral and broadband flir data fusion," in *Electro-Optical Remote Sensing*, vol. 5988, no. 1. Bruges, Belgium: SPIE, 2005, pp. 119–130.